CFD Simulation of Two Tandem Floating Offshore Wind Turbines in Surge Motion

CFD Simulation of Two Tandem Floating Offshore Wind Turbines in Surge Motion

Abdolrahim Rezaeiha[1,2], Daniel Micallef[3]

[1]KU Leuven, Leuven, Belgium.

[2]Eindhoven University of Technology, Eindhoven, The Netherlands.

[3]University of Malta, Msida, Malta.

Author contact email: a.rezaeiha@tue.nl; daniel.micallef@um.edu.mt

Keywords: offshore wind energy, floating wind turbine, wind farm design, wake interaction, aerodynamics, power performance

ABSTRACT

High-fidelity unsteady Reynolds-averaged Navier-Stokes (URANS) CFD simulation is employed to investigate the variations in the power performance of two tandem in-line floating offshore horizontal axis wind turbines for the scenario in which the upstream rotor is oscillating in surge motion and the downstream rotor is positioned in a distance of 3D (D: turbine diameter) and is stationary. The rotors are the NREL-5MW reference turbine. The platform surge period and wave amplitude are 9 s and 1.02 m, respectively. The results are presented for 100 full surge periods. It is found that the surge motion of the upstream rotor results in: (i) sinusoidal fluctuations in the power and thrust coefficients (C_P and C_T) of the upstream rotor with a standard deviation (std) of 9.7% and 5.5%, respectively; (ii) such fluctuations in C_P and C_T are less regular with a std of 4.2% and 2.8% for the downstream rotor, respectively. A low-frequency oscillating mode with a period nearly 10 times the surge period is also observed for the downstream rotor. The mean C_P and C_T of the downstream rotor are 28.9% and 38.5% of the upstream one.

1 Introduction

Floating offshore wind power has received wide attention in order to take advantage of the largely unexploited deep offshore wind potential. The technology is still hindered by high Levelized Cost of Energy (LCOE) (see Bosch et al. [5] and Kausche et al. [10]) and technological challenges such as those associated with mooring, electrical cables and floaters (see for example [3]). Rotor aerodynamics, despite the knowledge accumulated for the fixed rotor case, e.g. [18], reveals new challenges in view of the unsteady nature of the flow as is the case with floating platforms. Effectively a floating wind turbine rotor has six degrees of motion which are largely dependent on the coupled

wind-wave action. These result in highly complex 3D blade motions which further complicate the resulting wake flows [2]. Furthermore, in a continuous effort to upscale rotors beyond 15MW, new challenges can arise such as flow compressibility, addressed by Sørensen et al. [23] towards the blade tip which is not usually considered for even the largest (non-flying) machines in existence today.

While the problem of floating offshore wind turbines is a multi-physics one involving complex aero-hydrodynamic coupling, most of the research has been targeted at investigating the hydrodynamics and the aerodynamics in isolation with some assumed boundary conditions. Research articles on the wake aerodynamics of platform pitching motion by Wen et al. [26] reveal the influence on power with varied tip speed ratio and reduced frequency as a result of the pitching motion. They show that The power variation increases with increasing tip speed ratio and reduced frequency. Another article on the effect of platform pitching motion by Jeon et al. [9] using a vortex lattice method shows the presence of a turbulent wake state under low-speed inflow conditions. Another study by Tran et al. [24] investigates the effect of platform pitching motion on the unsteady aerodynamics of the rotor. Lin et al. [11] also report full body rotor Computational Fluid Dynamics (CFD) computations involving pitching and surging motion.

The research focus on floating offshore wind turbines has been mostly dedicated to surge motion in isolation. Some examples include Bayati et al. [2], Micallef and Sant [12], Farrugia et al. [7] and [6]. These authors investigate the wake and loading characteristics of floating offshore wind turbines at different tip speed ratios. Information such as transient inductions, angle of attack and loads has been reported numerically. Experiments such as Sant et al.[19] also report transient inductions using hot-wire measurements but in general there is a need for more experimental evidence of the wake behavior.

The approaches used for rotors on a fixed platform have found widespread use in floating offshore rotors. Blade Element Momentum (BEM) approaches have been used by Tran et al. [24] and Farrugia et al. [7]) with dynamic wake corrections such as by Pitt and Peters [14] and [22]. In view of the fact that the wake behavior is not directly modeled, such approaches have just been used as a code-to-code comparative analysis. Sant and Micallef show that these models do not compare well with more advanced methods [20]. The Generalized Dynamic Wake (GDW) method has also received some attention (see for instance Micallef and Sant [12]) in view of the fact that it considers the wake dynamics. Nonetheless, like BEM it has been mostly employed for comparative purposes rather than as a benchmarking tool. Despite this, the AeroDyn FAST solver [13] which employs both BEM and GDW can be used to couple the aerodynamics with the hydrodynamics which can hence resolve the platform dynamics. With this approach, under given wave amplitudes and frequencies, the platform motions can be established and used as inputs to investigate the wake aerodynamics. More advanced methods include the free-vortex, lifting-line methods such as that developed by Sebastian and Lackner [21]. Navier-Stokes based Actuator Disc (AD) and Actuator Line (AL) models have also been utilized in the literature such as by de Vaal et al.[6].

Studies on multiple floating wind turbines, as found in wind farms of the future, have found little attention particularly on the turbine-to-turbine wake interactions. Such studies are on the other hand common for rotors on a fixed platform, especially during the last decade (see for instance Troldborg [25]). One issue is that multiple floating turbines interacting with each other have coupled aero-dynamics, hydrodynamics and platform dynamics, and this dramatically increases the complexity of the analysis. The principal aim of the current work, however, is to study the variations in the aero-dynamic performance of two in-line floating horizontal axis wind turbines in a tandem arrangement oscillating in surge motion. Therefore, a decoupled aerodynamic analysis with a prescribed surge motion is performed. The surge motion characteristics are set based on previous work by the au-

thors [12]. The de-coupling simplicity provides us with the opportunity to focus on the aerodynamic interactions due to the surge motion. The analysis will focus on the variations in the turbines power and thrust coefficients where the upstream rotor is oscillating in surge motion and the downstream rotor is stationary.

The outline of the work is as follows. The details of the actuator disc modeling and the CFD simulations are given in Sec 2. The results are discussed in Sec. 3 and the conclusions are provided in Sec. 4.

2 Methodology

2.1 Overview of the methodology

The approach used to answer the main research question is based on numerical simulations of two tandem, in-line floating offshore wind turbines oscillating in surge motion for the following scenario: oscillating upstream turbine, stationary downstream turbine with 3D (D: turbine diameter) streamwise distance in between. Note that 5D distance is the more typical value in the farms, nevertheless, as the focus of the present study is on the wake interactions and the resultant oscillating power performance of the rotors, the smallest applicable distance is selected to ensure the maximum interactions.

In the present study, high-fidelity CFD simulations are performed, where the influence of the turbines on the flow field due to the rotor loading are taken into account using the actuator disc (AD) model coupled with the CFD simulation through a User Defined Functions (UDF).

The AD model, see Sec. 2.3, is coupled based on the work by Micallef and Sant [12] and Bezzina et al. [4]. In the present study, this model has been adapted to accommodate two tandem in-line rotors. The analysis is performed for a given surge amplitude and frequency, see Sec. 2.5.

2.2 Wind turbine characteristics

Table 1 lists the geometrical and operational characteristics of the National Renewable Energy Laboratory (NREL) 5MW reference wind turbine, which is used in the simulations. Figure 1 shows a schematic of the two tandem floating offshore wind turbines in surge motion. The turbines have a collective pitch angle of 0°.

2.3 Actuator disc model

The actuator disc model used for the two in-line rotors is based on the formulation by Micallef and Sant [12] and de Vaal et al.[6] but extended in the present study to accommodate two rotors. The rotor loading is modeled as a source term in the momentum equations. These forces are first established using the Blade Element Theory (BET). Due to the surging motion, the relative flow angle will vary with time in a transient manner. The velocity diagram is shown in Fig. 2 with the rotor surging downstream. The blue vectors represent the rotor velocities while the red vectors indicate the aerodynamic velocities. The relative flow velocity V_{rel} and the angle of attack α are used in conjunction with 2D airfoil polars to find the lift and drag forces and hence the thrust and torque acting on a particular radial element and correct for tip/root loss effects using a Prandtl correction [8]. These forces are input as momentum source terms (axial and tangential).

The rotor surge motions (position and velocity) are input as sinusoidal motions with given amplitudes X_j [m] and frequencies ω_j [rad/s], see Eq. 1 - 2, where $j = 1, 2$. Fig. 3 shows the rotor position

Table 1: Summary of NREL-5MW design characteristics.

Parameter	
Wind regime	IEC Class 1A
Rotor orientation	Upwind
Rotation	Clockwise
Control	Variable speed, pitch-regulated, yaw controlled
Cut-in wind speed	4 m/s
Cut-out wind speed	25 m/s
Rated wind speed	11.4 m/s
Rated rotor speed	1.267 rad/s
Rated power	5.0 MW
Rated tip speed	90 m/s
Number of blades	3
Rotor diameter	126.0 m
Hub diameter	3.0 m
Hub height	90.0 m

and velocity for the oscillating upstream rotor (rotor 1) and the stationary downstream rotor (rotor 2).

$$x_j(t) = X_j sin\omega_j t \tag{1}$$

$$u_{s,j}(t) = X_j \omega_j cos\omega_j t \tag{2}$$

For convergence issues, the imposed aerodynamic forces are blurred using a Gaussian function to avoid issues of singularities, which might lead to solution divergence. This is given by Eq. 3:

$$\eta = \frac{1}{\epsilon\sqrt{\pi}} \exp \frac{-r^2}{\epsilon} \tag{3}$$

The ϵ_i is a scaling factor, see Eq. 4, and according to de Vaal et al.[6] should be $1 \leq \epsilon_i \leq 2$. Micallef and Sant [12] found 2.5 as a proper choice, also used here.

$$\epsilon = \epsilon_i \Delta x \tag{4}$$

The source term vector is applied by convoluting the force **F** and divided by the volume of each annular element ΔV.

$$\mathbf{S} = \frac{\int_{-\infty}^{\infty} \mathbf{F} * \eta dx}{\Delta V} \tag{5}$$

The main assumption used in the current model is that the platform motions of both turbines are treated in a decoupled manner as a first approximation in order to limit down the complexity of

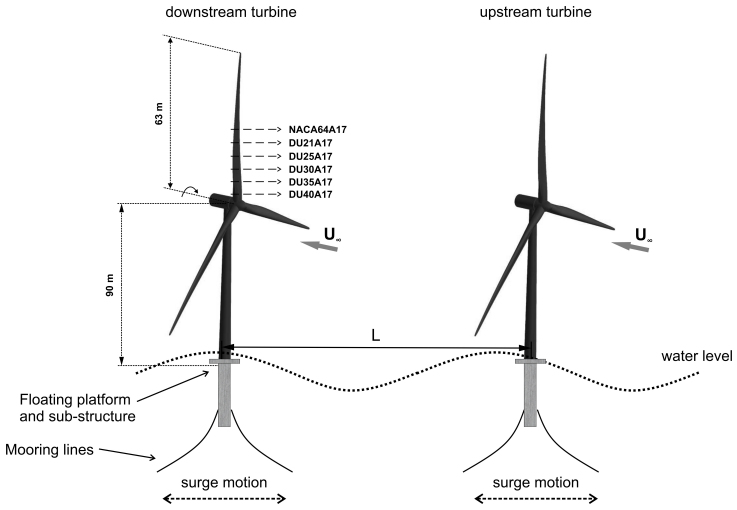

Figure 1: Schematic of two tandem floating rotor configuration in surge motion.

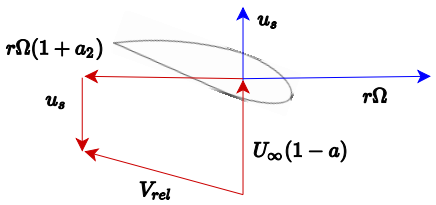

Figure 2: Velocity diagram for a blade section of a surging rotor.

hydrodynamic and dynamic effects. In reality, the platform motions of the downstream turbine will not be identical to that of the upstream turbine due to the wake interference effects, which will somewhat alter to system dynamics. The iterative methodology is given in the flowchart, see Fig. 4.

2.4 CFD computational settings

2D axisymmetric incompressible unsteady Reynolds-Averaged Navier Stokes (URANS) simulations are performed. The commercial CFD software package ANSYS Fluent v16.1 [1] is used. The computational domain size is $28D \times 10D$ where D is the turbine diameter. The distance from the upstream turbine to the domain inlet is $5D$. A fully-structured computational grid with refinement in the rotor region and the wake area is generated, see Fig. 5. The total number of cells is 75,152 cells with 63 cells along the blade radius. The boundary condition at the domain inlet and outlet is uniform velocity inlet and zero static gauge pressure outlet and the domain top side is symmetry (slip) wall. Turbulence is modeled using the two-equation SST $k-\omega$ model. The model is shown to give accurate predictions of aerodynamic performance of wind turbines in different operating regimes, from optimal to dynamic stall, in comparison against experimental data and more complex scale-resolving simulation approaches, see [16, 15, 17]. SIMPLE pressure-velocity coupling scheme is employed. The time step is 0.04 s with 20 iterations per time step.

The simulations procedure is as follows. The steady RANS simulation is performed to have converged solution for 2 steady rotors. The solution is employed to initialize the transient simulation, where the upstream rotor is oscillating in surge motion with the amplitude and period given in Sec. 2.5.

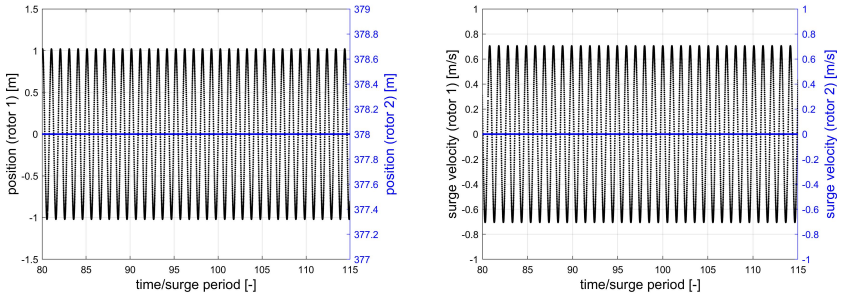

Figure 3: Rotor position and velocity for the oscillating upstream rotor (rotor 1) and the stationary downstream rotor (rotor 2).

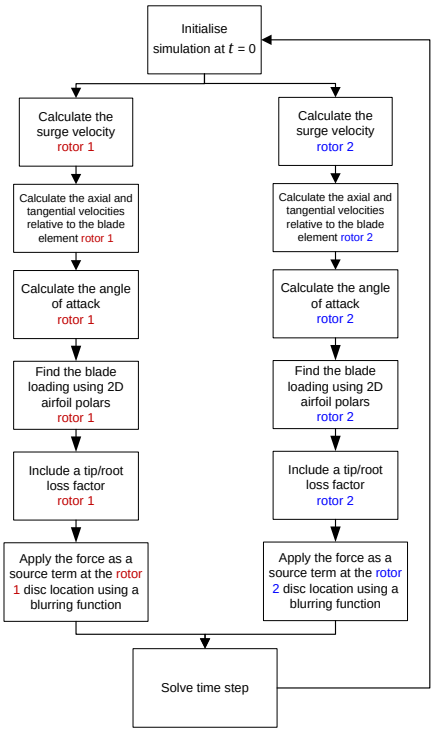

Figure 4: Overall view of the iterative approach for the calculation of aerodynamic loading of the two rotors using the actuator disc model coupled with CFD.

The transient simulation continues for 15 full surge periods to reach statistical convergence. The presented results correspond to 100 full surge periods, i.e. 15 - 115.

2.5 Test matrix

The test matrix, given in Table 2, provides the details of the surge motion for the upstream rotor and the rotor settings for both rotors. The reference wind speed refers to the value employed in BEM calculations to calculate the relative velocity and the angle of attack.

Note that as shown in Sec. 3, the downstream rotor is experiencing much lower incident-flow velocity, i.e. 5.5 m/s. Therefore, its rotor settings is set differently than the rated conditions to

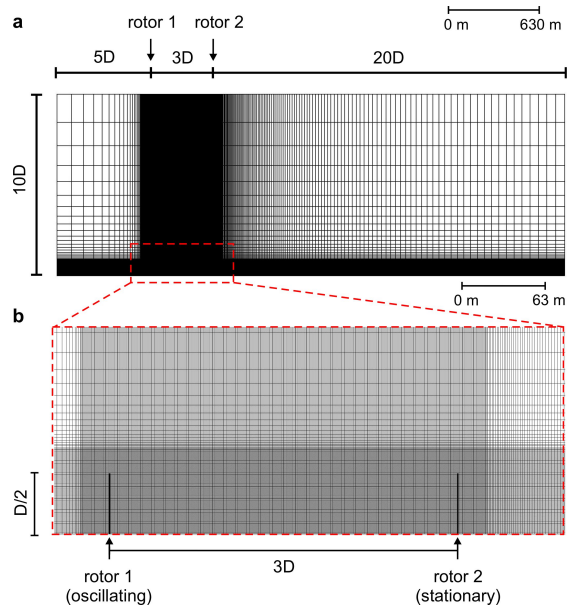

Figure 5: Computational domain and grid for the CFD simulation.

operate optimally and it has a rotor speed of 0.84 rad/s according to the NREL design curve, see Table 2. Thus, as obvious, the two rotors are not operating with the same rotor speed and tip speed ratio.

Table 2: Platform surge motion characteristics and the rotors settings (tip speed ratio λ and rotor speed Ω). The subscripts 1 and 2 denote the upstream and downstream rotors, respectively.

Amplitude, A [m]	Period [s]	Frequency [Hz]	Distance between rotors	U_∞ [m/s]	λ_1	λ_2	Ω_1 in rad/s (in Hz)	Ω_2 in rad/s (in Hz)
1.02	9.00	0.11	3D	11.40	7.00	9.62	1.267 (0.2)	0.84 (0.13)

3 Results

Fig. 6 shows the time-averaged contour plots of the pressure coefficient and normalized velocity magnitude for the streamwise positions x/D = -1 - 10, with respect to the upstream rotor. It can be seen that due to the small distance between the two rotors, the incident-flow for the downstream rotor is on average significantly dropped due to the wake of the upstream rotor. The area-weighted average velocity along the rotor span is nearly 5.5 m/s. As indicated in Sec. 2.5 and table 2, hence the downstream rotors settings are adjusted according to the NREL design curve.

Fig. 7 shows the variations of the thrust force and torque of the two rotors in 45 full surge periods. Fig. 8 shows the thrust and power coefficients (C_T and C_P) of the two turbines normalized with the mean coefficient values of the upstream rotor. Fig. 9 shows the spatiotemporal contour plots of angle of attack, thrust force and torque for the oscillating upstream rotor (rotor 1) and the stationary downstream rotor (rotor 2).

A first observation is that the thrust and torque of the upstream rotor vary in a quasi-sinusoidal manner with some noise at the maximum and minimum positions of the surging rotor. The reason

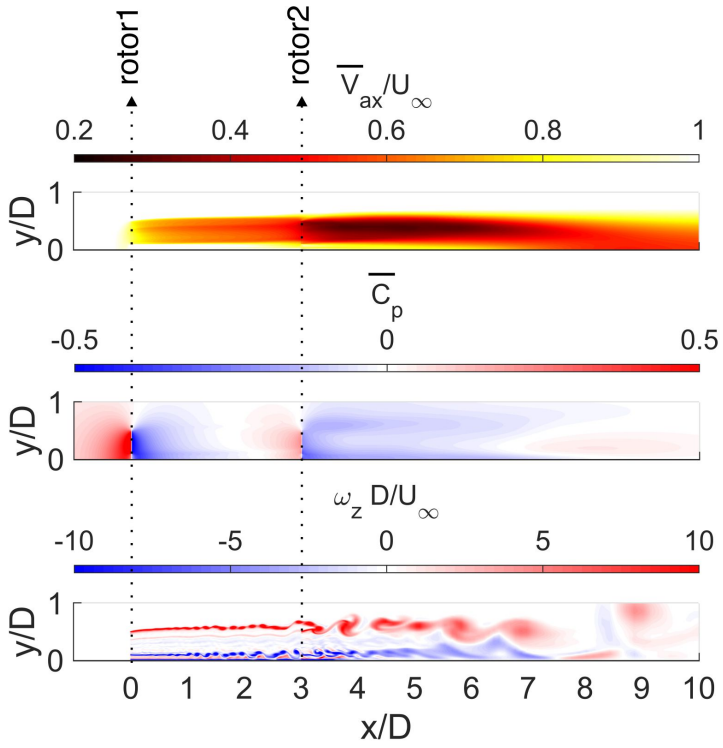

Figure 6: Dimensionless (time-averaged) axial velocity and pressure, (instantaneous) vorticity fields.

for these are the sudden changes in loads also shown in Fig. 9 occurring every $\frac{1}{2}$ surge period. The angle of attack, the spanwise distribution of normal and tangential forces of the upstream rotor are noticeably different during the fore and aft motions of the rotor.

The oscillatory behavior of the upstream rotor loading has 180° phase difference with the rotor surge speed, meaning that the maximum thrust force and torque corresponds to the most negative surge velocity (when surging upstream). This is expected considering the velocity diagram shown in Fig. 2.

The C_P and C_T values of the surging upstream rotor have a standard deviation of 9.7% and 5.5%, respectively.

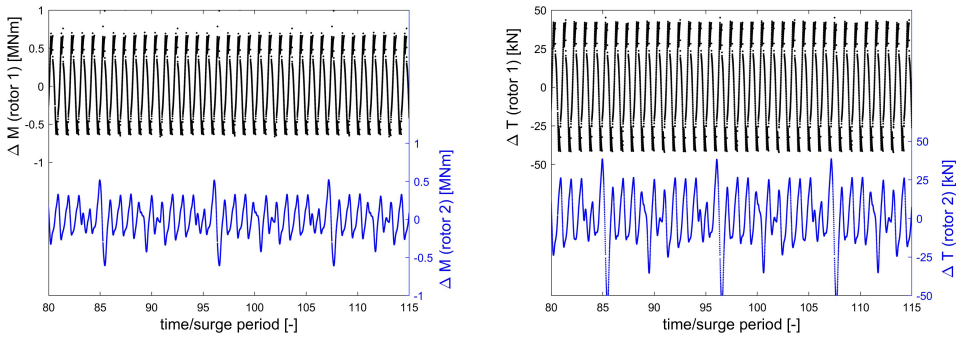

Figure 7: Variations of the thrust force and torque for the oscillating upstream rotor (rotor 1) and the stationary downstream rotor (rotor 2).

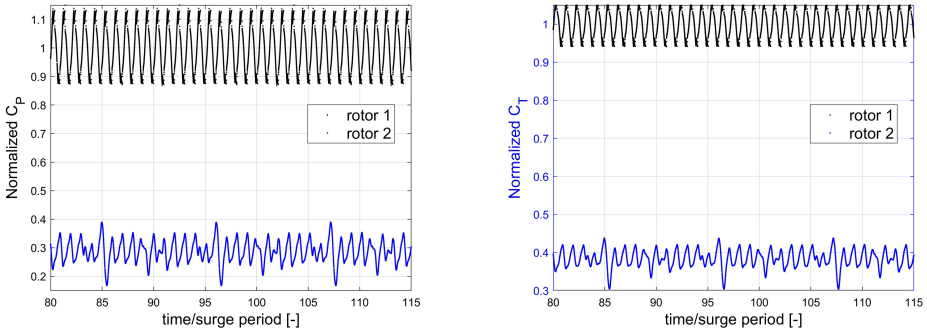

Figure 8: Normalized thrust and power coefficients for the oscillating upstream rotor (rotor 1) and the stationary downstream rotor (rotor 2).

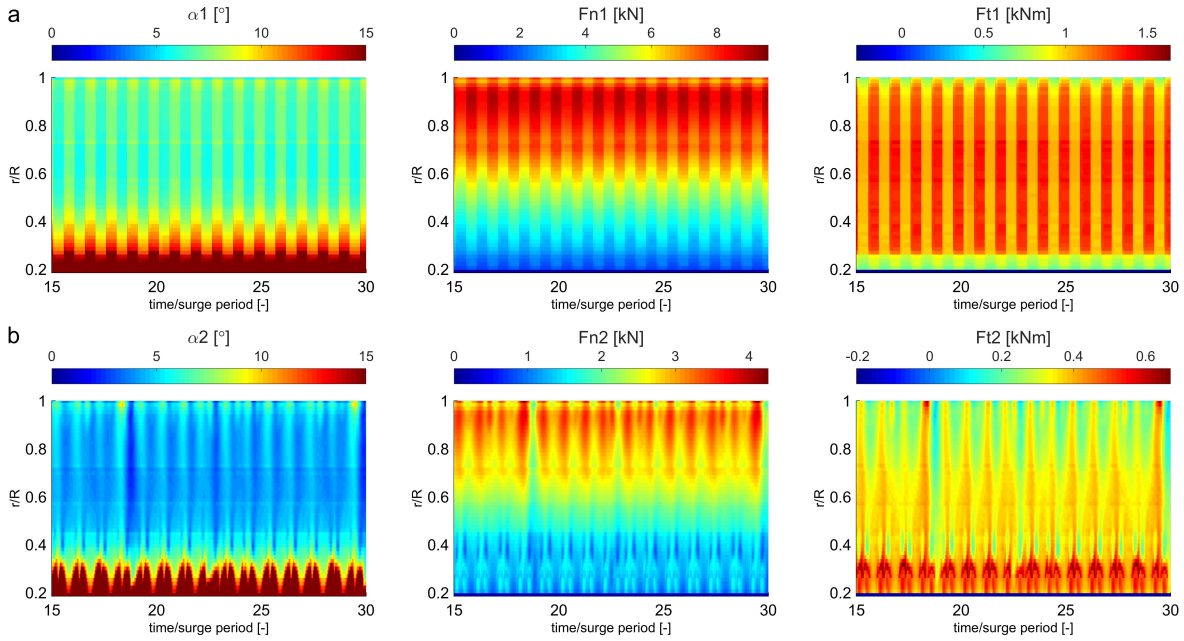

Figure 9: Spatiotemporal contour plots of angle of attack, thrust force and torque for (a) the oscillating upstream rotor (rotor 1) and (b) the stationary downstream rotor (rotor 2).

The surge motion of the upstream rotor significantly influences the thrust force and torque of the stationary downstream rotor located 3 rotor diameter downstream. The fixed downstream rotor experiences a non-sinusoidal behavior due to the resulting wake dynamics of the upstream rotor. The behavior of the oscillating loads of the downstream looks more complex with more harmonics of different frequencies other than only the surge frequency, due to wake interactions. Frequency analysis of the instantaneous C_P and C_T signals of the two rotors shown in Fig. 10, however, reveals that the dominant frequency for both upstream and downstream rotors is still the surge frequency, i.e. 0.11 Hz. For the downstream rotor, moreover, a low-frequency oscillating mode with a period nearly 10 times the surge period is also observed. Further analysis of this low-frequency mode is considered for future research. Note that the frequency analysis is based on the time series for 100 full surge periods.

The mean C_P and C_T of the stationary downstream rotor are 28.9% and 38.5% of the upstream

one and have a standard deviation of 4.2% and 2.8%, respectively.

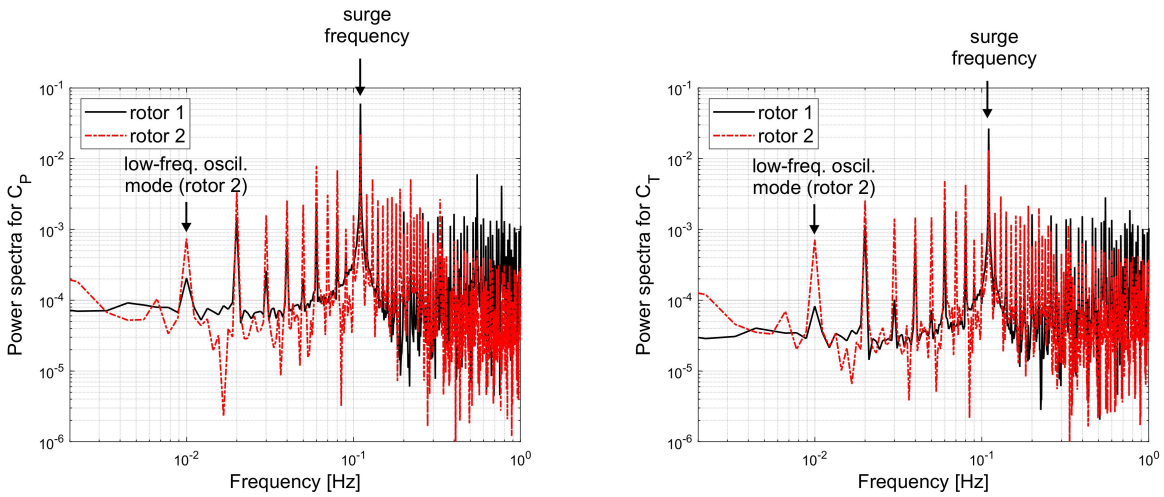

Figure 10: Power spectra of the oscillating power and thrust coefficients of the two rotors.

Fig. 11 shows the spanwise distribution of the normal and tangential loads for the oscillating upstream rotor and the stationary downstream rotor. In addition to substantially lower normal and tangential forces observed on the downstream rotor, its spanwise normal force distribution is found to be much more uniform than the upstream rotor, and has comparatively limited variations from root to tip. The tangential load distribution of the downstream rotor also decays in the outer spanwise extent of the blade for $r/R > 0.7$ due to the wake of the upstream rotor.

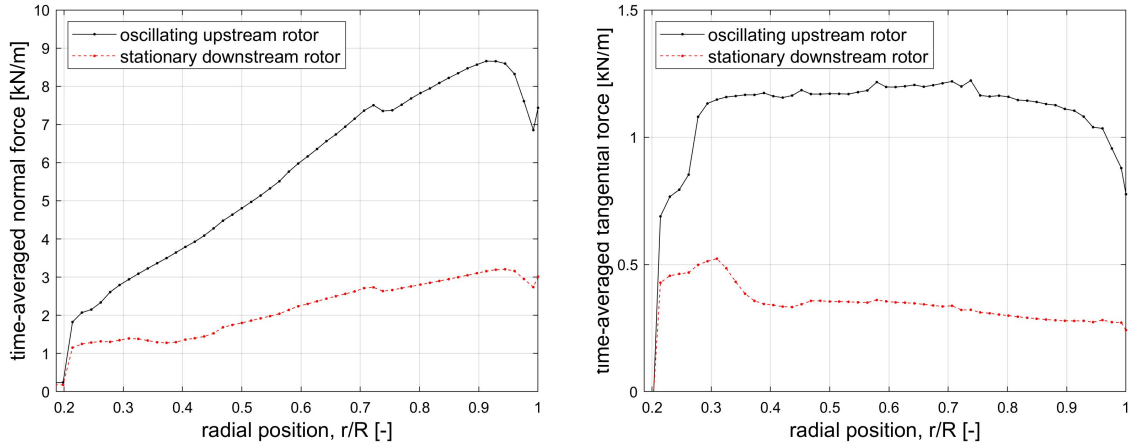

Figure 11: Spanwise distribution of normal and tangential loads for the oscillating upstream rotor (rotor 1) and the stationary downstream rotor (rotor 2) in the last time step.

4 Conclusions

The following conclusions can be drawn from this study:

- Thrust and torque of the upstream rotor vary quasi-sinusoidally, due to the imposed sinusoidal surge motion of the rotor, with some discontinuities at the maximum and minimum peaks.

- The thrust and torque of the downstream rotor is directly influenced by the wake dynamics of the upstream rotor in a non-sinusoidal manner.
- frequency analysis of the turbine forces reveal the dominance of the surge frequency for both upstream and downstream rotors.
- The C_P and C_T values of the surging upstream rotor have a standard deviation of 9.7% and 5.5%, respectively.
- The mean C_P and C_T of the stationary downstream rotor are 28.9% and 38.5% of the upstream one and have a standard deviation of 4.2% and 2.8%, respectively.

5 Acknowledgments

The 1st author is currently a postdoctoral fellow of the Research Foundation Flanders (FWO) and is grateful for the financial support (project FWO 12ZP520N).

References

[1] ANSYS. ANSYS Fluent Theory Guide. Technical Report Release 15.0, ANSYS Inc., Canonsburg, PA, 2013.

[2] I. Bayati, M. Belloli, L. Bernini, D.M. Boldrin, K. Boorsma, M. Caboni, M. Cormier, R. Mikkelsen, T. Lutz, and A. Zasso. UNAFLOW project: UNsteady aerodynamics of FLOating wind turbines. *Journal of Physics: Conference Series*, 1037:072037, 2018.

[3] Nuno Bento and Margarida Fontes. Emergence of floating offshore wind energy: Technology and industry. *Renewable and Sustainable Energy Reviews*, 99:66–82, 2019.

[4] Ryan Bezzina, Tonio Sant, and Daniel Micallef. Modelling the Aerodynamics of a Floating Wind Turbine Model Using a CFD-Based Actuator Disc Method. pages 1–12, 2019.

[5] Jonathan Bosch, Iain Staffell, and Adam D Hawkes. Global levelised cost of electricity from offshore wind. *Energy*, 189:116357, 2019.

[6] J B de Vaal, M O L Hansen, and T Moan. Effect of wind turbine surge motion on rotor thrust and induced velocity. *Wind Energy*, 17(1):105–121, 2014.

[7] R. Farrugia, T. Sant, and D. Micallef. A study on the aerodynamics of a floating wind turbine rotor. *Renewable Energy*, 86:770–784, 2016.

[8] H.e Glauert. *Aerodynamic Theory*. Dover: New York, 169-360, 1963.

[9] Minu Jeon, Seungmin Lee, and Soogab Lee. Unsteady aerodynamics of offshore floating wind turbines in platform pitching motion using vortex lattice method. *Renewable Energy*, 65(0):207–212, 2014.

[10] Michael Kausche, Frank Adam, Frank Dahlhaus, and Jochen Großmann. Floating offshore wind - Economic and ecological challenges of a TLP solution. *Renewable Energy*, 126:270–280, 2018.

[11] Lin Lin, Kai Wang, and Dracos Vassalos. Detecting wake performance of floating offshore wind turbine. *Ocean Engineering*, 156:263–276, 2018.

[12] Micallef, D. and Sant, T. Loading effects on floating offshore horizontal axis wind turbines in surge motion. *Renewable Energy*, 83:737–748, 2015.

[13] P J Moriarty. AeroDyn Theory Manual. (January), 2005.

[14] Dale M. Pitt and David A Peters. THEORETICAL PREDICTION OF DYNAMIC-INFLOW DERIVATIVES. (47), 1980.

[15] A. Rezaeiha, H. Montazeri, and B. Blocken. Cfd analysis of dynamic stall on vertical axis wind turbines using scale-adaptive simulation (sas): Comparison against urans and hybrid rans/les. *Energy Conversion and Management*, 196(C):1282–1298, 2019.

[16] A. Rezaeiha, H. Montazeri, and B. Blocken. On the accuracy of turbulence models for cfd simulations of vertical axis wind turbines. *Energy*, 180(C):838–857, 2019.

[17] A. Rezaeiha, H. Montazeri, and B. Blocken. *Scale-Adaptive Simulation (SAS) of dynamic stall on a wind turbine*, volume 143, pages 323–333. Springer International Publishing, 1 edition, 2020.

[18] A. Rezaeiha, R. Pereira, and M. Kotsonis. Fluctuations of angle of attack and lift coefficient and the resultant fatigue loads for a large horizontal axis wind turbine. *Renewable Energy*, 114(B):904–916, 2017.

[19] T. Sant, D. Bonnici, R. Farrugia, and D. Micallef. Measurements and modelling of the power performance of a model floating wind turbine under controlled conditions. *Wind Energy*, 18(5):811–834, may 2015.

[20] Tonio Sant and Daniel Micallef. Disparity Analysis for Three Floating Wind Turbine Aerodynamic Codes in Comparison. pages 1–10, 2019.

[21] T Sebastian and M A Lackner. Development of a free vortex wake method code for offshore floating wind turbines. *Renewable Energy*, 46(0):269–275, 2012.

[22] H Snel and J G Schepers. Joint investigation of dynamic inflow effects and implementation of an engineering method. Technical report, 1995.

[23] Niels Sørensen, Franck Bertagnolio, Eva Jost, and Thorsten Lutz. Aerodynamic effects of compressibility for wind turbines at high tip speeds. *Journal of Physics: Conference Series*, 1037:22003, 2018.

[24] Thanhtoan Tran, Donghyun Kim, and Jinseop Song. Computational Fluid Dynamic Analysis of a Floating Offshore Wind Turbine Experiencing Platform Pitching Motion. pages 5011–5026, 2014.

[25] Niels Troldborg. *Actuator Line Modeling of Wind Turbine Wakes*. Phd, Technical University of Denmark, Copenhagen, 2009.

[26] Binrong Wen, Xingjian Dong, Xinliang Tian, Zhike Peng, Wenming Zhang, and Kexiang Wei. The power performance of an offshore floating wind turbine in platform pitching motion. *Energy*, 154:508–521, 2018.